A parametric analysis of salp-like propulsion

Hannes Aspåker

June 9, 2021

Abstract

Salps are barrel shaped aquatic invertebrates, which swim by jet propulsion. Despite their abundance they remain relatively understudied, and previous studies of jet propulsion among salps have given imprecise and sometimes contradictory results. To better understand the possibility of numerical simulation as a tool to analyse this jet propulsion, the fluid dynamics of a test case consisting of a simplified model of a two-dimensional salp is simulated using a finite element approximation. The results are compared with physical measurements from previous studies. A parametric analysis is made where thrust is analysed as a function of posterior siphon diameter and maximum chamber height, and an exponential relationship is found in both cases. Several possibilities and limitations are discovered which could guide the design of future more detailed studies.

1 Introduction

1.1 Background

Salps are barrel shaped, gelatinous invertebrates found in the ocean, which swim by jet propulsion [1]. Despite their abundance – during a swarm they can constitute 99% of the zooplankton community (by biomass) and cover an area up to 100 000 km^2 - they remain relatively understudied [2].

In salps, jet propulsion begin by taking in water via the anterior (front) siphon to fill its mostly hollow body. Next, circular muscle bands around its body contract to force a jet of fluid out of the posterior siphon. This process is then repeated to create a rhythmic forward movement [1]. This is illustrated in figure 1.

The jet propulsion of salps is known to be the most efficient example of jet propulsion in the animal kingdom [3]. In fact, salps do well even when compared to other modes of locomotion, such as swimming fish [4]. This combination of efficiency and simplicity makes salps an interesting object of study in the context of underwater propulsion. For example, Salps have repeatedly been used as inspiration in the design of small underwater vehicles [5] [6] [7].

Salps have long been known to use vortex ring propulsion [1] [3], where the pulsed jets form toroidal vortices behind the salp. The pulses incorporate extra mass as they roll into vortices, which results in a pulsed jet being more efficient than a continuous jet of the same magnitude [3]. Each pulse result in a single vortex, and consecutive jets are spaced such that there is no interaction between vortex rings [1]. The frequency of pulsing is around 0.5-2.5 Hz [3].

Another unique property of salp locomotion is their ability to easily reverse the direction of movement by switching the role of the anterior and posterior siphon, which is used to quickly escape from sudden threats [1].

The Reynold's number for swimming salp range from 150 to 6000 depending on organism size [3]. These values fall within the range where streamlining is important to reduce flow separation and pressure drag, which could explain the relatively streamlined bodies of salp [3].

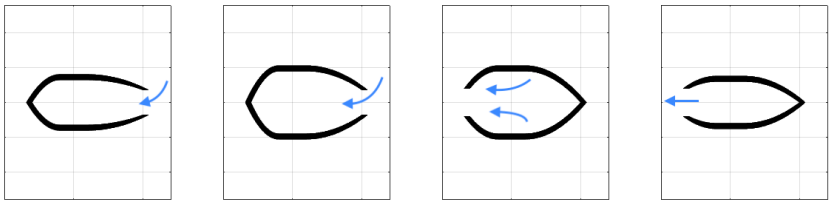

Figure 1: An illustration showing the salp jet cycle.

1.2 Research question

Many previous measurement techniques of salp motion has suffered from being either inexact, invasive or both. Studies have giving conflicting results [1], and accurate measurements of free-swimming salps have also proven to be challenging [8]. A numerical analysis of salp motion, using a theoretical model of a salp, could therefore be a valuable tool to improve our understanding of the salp jet cycle.

The aim of this report is to explore the feasibility of numerical analysis of salp-like propulsion, by implementing and analysing a test case consisting of a simplified model of a two-dimensional salp. The jet cycle is analysed and a parametric analysis of forward thrust versus siphon diameter and chamber height is performed. Discovered limitations and possiblites could guide future more detailed studies.

1.3 State of the art

Few studies have been made of salp swimming kinematics [1], and none using numerical simulation. Previous studies have used either physical measurements, or computer aided analysis of recorded video using fluorescent dyes or particle image velocimetry. As mentioned, some studies have given conflicting results [1].

Sutherland *et al.* have studied (via measurement and particle image velocimetry) how body morphology affect the swimming kinematics of different species of salp [1], including estimations of thrust and jet velocity. Bone *et al* have studied the pressure, thrust and jet velocity of a single species of salp (*Salpa fusiformis*).

2 Method

2.1 Parameterizion of salp body

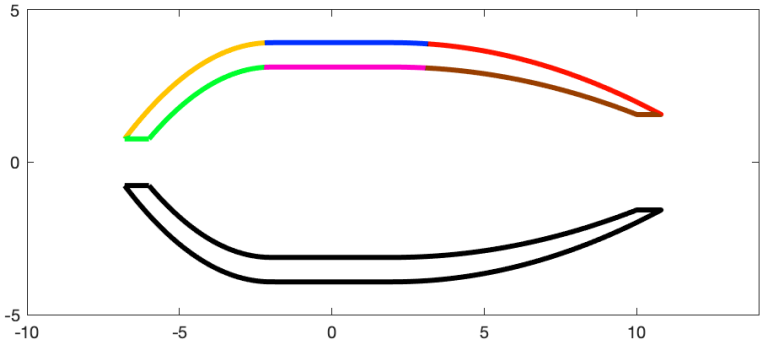

Figure 2: A mathematical representation of the salp body, consisting of an upper mantle and a lower mantle. The sections corresponding to different functions (quadratic and linear) of the upper mantle are shown with different colors.

We create an idealized representation of the salp body in two dimensions, consisting of an upper section (upper mantle) and a lower section (lower mantle), as in figure 2. Each section consists of two curves, joined to form a continuous shape, with each curve being a combination of two quadratic functions connected by a straight line, as in equation 1.

$$y = \begin{cases} a \cdot b_1(-(x+l)^2 + h + c_1) & \text{if } -(l+r_1) \leq x < -l \\ a \cdot h & \text{if } -l \leq x \leq l \\ a \cdot b_2(-(x+l)^2 + h + c_2) & \text{if } l < x < (l+r_2) \end{cases} \tag{1}$$

.

The parameter l in equation 1 represents half the length of the straight line, while the parameters r_1 and r_2 represent the length of left (posterior) and right (anterior) curved sections, respectively. the parameter h represents the height of the salp in the contracted state ($a = 1$). The parameter a is a general scaling that can be used to contract and expand the body, with $a = 1$ representing full contraction and values $a > 1$ representing expansion. The parameters $b_{1,2}$ and $c_{1,2}$ can be calculated as in equations 2 and 3, where d_1 and d_2 represent the radius of the left (posterior) and right (anterior) openings, respectively. The length and height of the upper curve is shifted using a thickness parameter θ to achieve a distance between the upper and lower curve and a thus a corresponding thickness to the mantle.

$$c_1 = \frac{d_1 \cdot h + r_1^2 h - h^2}{h - d_1} \tag{2}$$

$$b_1 = \frac{h}{h + c_1} \tag{3}$$

.

Note that the lower mantle is simply the upper mantle mirrored through the vertical center line. Movement of the salp, such as contraction and expansion, is implemented by specifying the parameters as continuous functions in time. This allows a cyclic movement as in figure 1 to be implemented.

2.2 Finite element approximation

The fluid was simulated by solving the Navier-Stokes equations using a stabilized space-time finite element method, finding a velocity u and pressure p that satisfies the variational formulation

$$(\dot{u} + (u \cdot \nabla)u, v) - (p, \nabla \cdot v) + (\nu \nabla u, \nabla v) + (\nabla \cdot u, q) + SD(u, p; v, q) = 0,$$

for all test functions v and q on the domain Ω, with u, p, v, q as piecewise linear polynomials. Here, $SD(u, p; v, q)$ is a residual based stabilization term as described by Hoffman *et al* [9].

The above variational formulation was semi-discretized in space and time, using trapezoidal time stepping. The time step was chosen to satisfy the CFL condition according to the local velocity and mesh diameter,

$$\Delta t = \min_{\Omega} \frac{1}{2} \frac{h}{|u^{\text{prev}}|}$$

where h is the local mesh diameter and $|u^{\text{prev}}|$ is the local velocity magnitude of the previous time step. In cases of sudden and large movements of the salp body, the time step was further restricted to give a maximum change of 2% in the salp body parameters between steps.

The horizontal force F on the boundary Γ of the salp's body is calculated using Green's formula according to

$$F(u, p, \phi) = < \nu \nabla u \cdot n - pn, \Phi >_{\Gamma} = \ (\dot{u} + (u \cdot \nabla)u, \Phi) + (\nu \nabla u, \nabla \Phi) - (p, \nabla \cdot \Phi),$$

with $\phi = (1, 0)$, corresponding to the horizontal direction.

2.3 Mesh

A large domain (relative to the size of the salp) is implemented to minimize the effect of the domain boundary on the investigation of the salp, using a very course mesh toward the edges of the domain to reduce computational time. The mesh is refined around the body of the salp, with maximum refinement at the area around the posterior siphon where we expect vortex formation, as seen in figure 3. The body of the salp is implemented as a hole in the mesh interior. To simulate movement of the salp, the boundary of the salp has a prescribed motion in time, with the mesh deforming around the salp using an elastic deformation model.

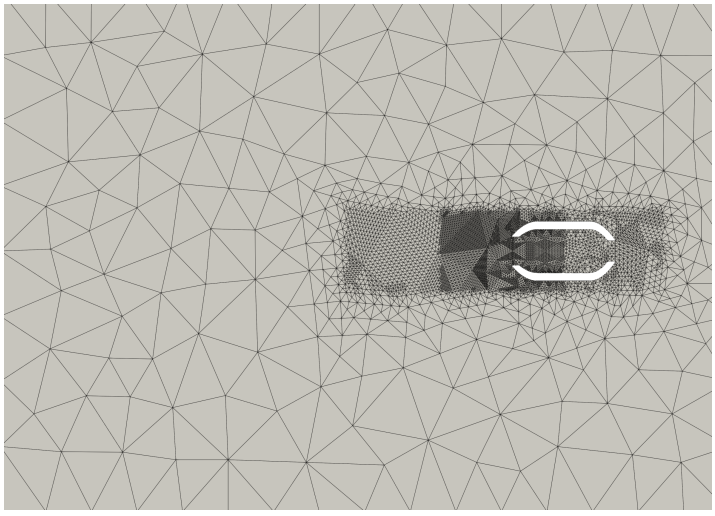

Figure 3: The mesh used in the finite element approximation.

2.4 Boundary conditions

To create conditions similar to open water, a zero-pressure ($p = 0$) Dirichlet boundary condition is set on the edges of the domain, far away from the salp. A no-slip boundary condition is implemented on the boundary of the salp body. Since the boundary will move over time, the no-slip condition is not equivalent to zero velocity, but rather a velocity equal to the movement of the boundary, in the direction normal to the boundary facet. If a point is prescribed a vertical displacement Δy at a timestep of size Δt, the boundary velocity v is set as

$$\begin{cases} v_x = \frac{n_x}{n_y} \frac{\Delta y}{\Delta t} \\ v_y = \frac{\Delta y}{\Delta t} \end{cases}$$

where $\vec{n}$ is the normal vector of the local facet. Since the boundary is defined by functions on the form $y = f(x)$, the displacement of each boundary point will always be specified in the vertical direction only.

2.5 Contact model

Contact between opposite ends of a siphon should close the siphon, preventing fluid flow between the interior and exterior of the salp. This is implemented via a remesh which joins both ends to form a continuous boundary when they are sufficiently close together (less than 0.25 mm), as seen in figure 4. The velocity and pressure field is copied to the new mesh using interpolation. To preserve the elastic deformation at the siphon when it switches back to an open position, the original mesh with an open siphon is kept in the background and updated simultaneously with the closed mesh as the salp deforms, such that a complete remesh can be avoided when switching back to the open position.

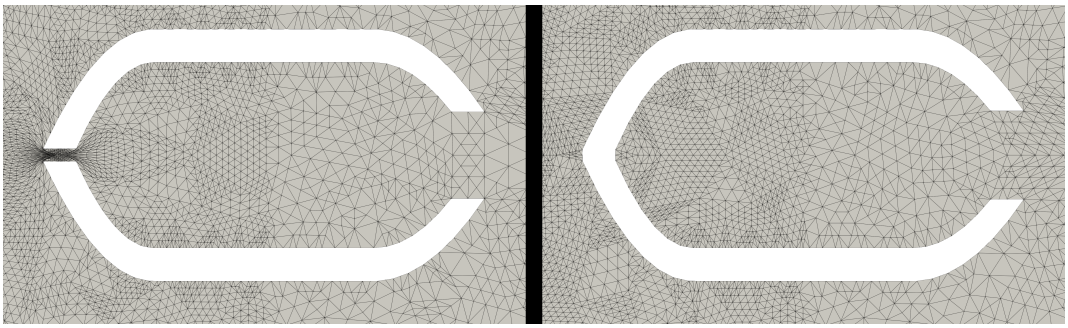

Figure 4: Comparison between open siphon (left image) and closed siphon following a remesh (right image).

2.6 Measurements

Thrust over a complete jet cycle and exhalent vortex velocity are measured for a model of *Salpa fusiformis*. The model (seen in figure 4) had a length of 1.7 cm, a contracted height of 60mm, an expanded height of 84mm, a posterior siphon diameter of 40mm, a pulse frequency of 1 Hz and a contraction time of 100 ms, in line with measurements taken by Bone et al [8]. The thrust measurement is taken at the last of three jet cycles, to ensure a steady-state measurement.

To investigate the relationship between posterior siphon diameter and thrust, the diameter is varied from 16mm to 56mm, with the mean thrust over a complete jet cycle being measured at each diameter.

To investigate the relationship between chamber size (or exhaled volume) and thrust, the size of the full chamber is varied from a height of 63mm to a height of 102mm, with the mean thrust over a complete jet cycle being measured at each size. The minimum height of the chamber (in the fully contracted state) is kept at 60mm in all circumstances.

3 Results

3.1 Jet cycle

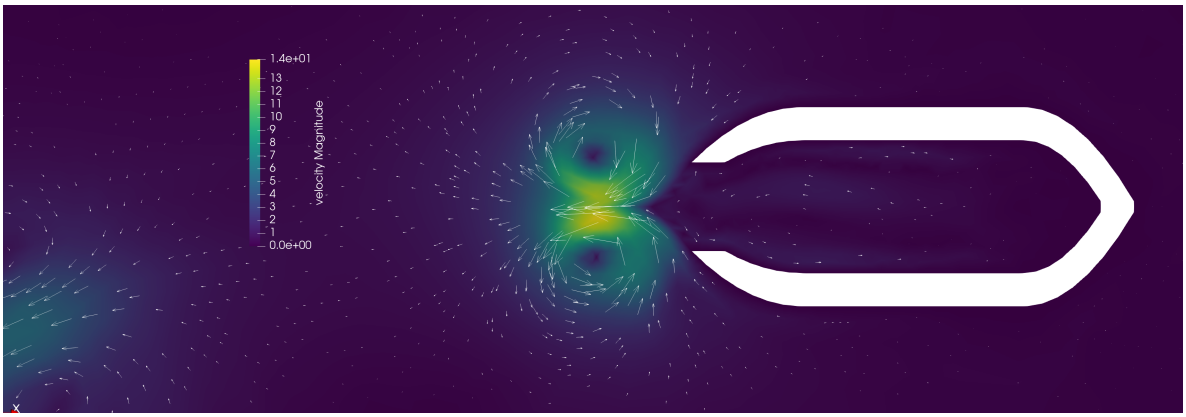

Figure 5: Vortex formation during the contraction step in the jet cycle.

The vortex formation during a jet cycle can be seen in figure 5.

The propulsive force as measured over two jet cycles can bee seen in figure 6. The average thrust was $3.17 \cdot 10^{-4}$ N. The exhalent vortex velocity was measured as 3.7 cm/s. The maximum pressure inside the chamber during contraction was measured as 660 Pa.

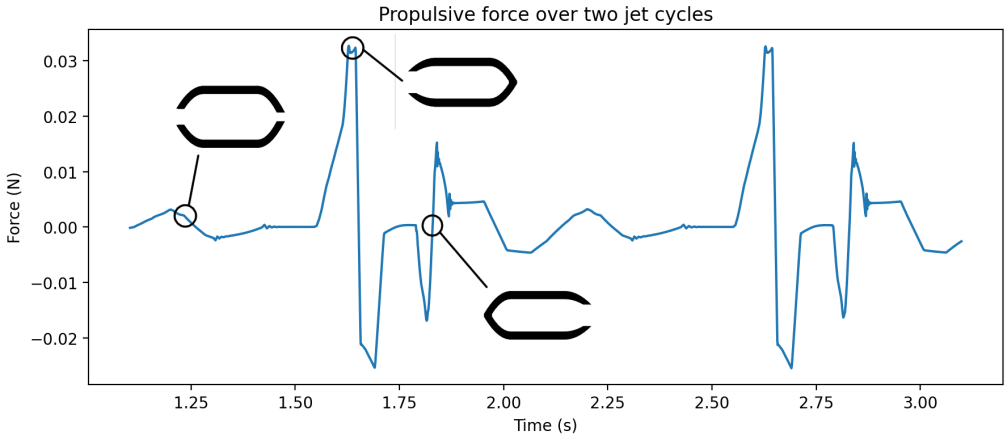

Figure 6: Posterior siphon diameter vs. mean thrust over a complete jet cycle. The shape of the salp at three points in time is overlayed on the curve.

3.2 Thrust versus siphon diameter

Average thrust as a function of posterior siphon diameter can be seen in figure 7. An exponential function has been fitted to the line using weighted linear regression, giving a function where the average thrust τ (in Newtons) depends on the diameter d (in centimeters) as

$$\tau = \exp\left(-(5.04 + 8.76d)\right).$$

3.3 Thrust versus chamber height

Average thrust as a function of maximum chamber high (corresponding to a larger chamber volume before contraction) is shown in figure 8.

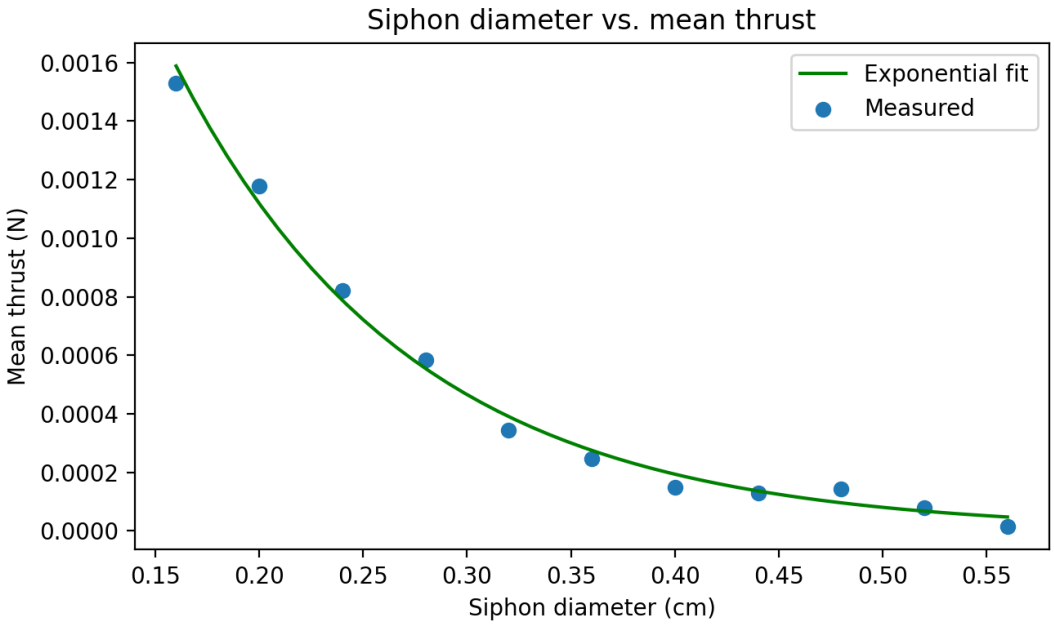

Figure 7: Average thrust vs siphon diameter

An exponential function has been fitted to the line using weighted linear regression, giving a function where the average thrust τ (in Newtons) depends on the height h (in centimeters) as

$$\tau = \exp\left(-11.6 + 12.6(h - 0.6)\right).$$

4 Discussion

4.1 Jet cycle

4.1.1 Comparison with previous studies

Bone *et al* [8] has previously measured the internal pressure and exhalent jet velocity of *Salpa fusiformis*. However, our measured velocity of 3.7 cm/s differs from Bone *et al* by an order of magnitude, who measured 22.8 cm/s. The measured pressure of 660 Pa differs from measurements of 60-100 Pa by Bone et al by an order of magnitude in the other direction.

However, Sutherland *et al* [1] noted an exhalent velocity of around 3 cm/s for many salps, which agrees well with our result. A more detailed comparison with the results measured by Sutherland is difficult due to the lack of details regarding the pulse cycle of the salps studied.

Sutherland also comments on the measurements made by Bone, noting that the measurements obtained could be unreliable due to the invasive measurements techniques used.

The pressure measured by Bone could also vary due to the location or time interval of the measurements, since the pressure varies substantially inside the chamber and decays rapidly with time.

Both Bone *et al* and Sutherland *et al* measured the thrust produced by the jet cycle, but comparisons with our results are difficult due to our measurements being taken in a two-dimensional plane, rather than on the full salp.

4.1.2 Jet cycle analysis

An interesting aspect of the jet cycle shown in figure 6 is the dip in thrust immediately following the peak thrust of the contraction. During the dip the thrust goes negative, giving a backwards acceleration. It is clear from the plot in figure 6 that this backwards thrust constitute a substantial reduction in the total (forward) thrust achieved during the cycle.

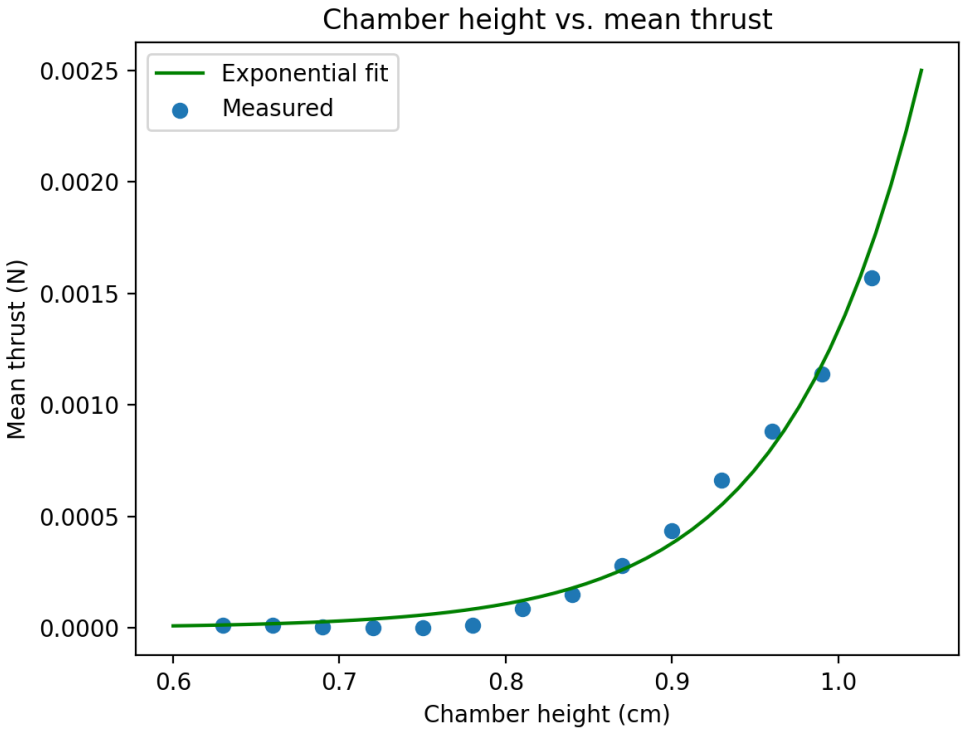

Figure 8: Average thrust versus maximum chamber height

During the peak thrust, we have a positive pressure gradient inside the salp - resulting in forward thrust. This pressure gradient is the result of the contraction of the salp forcing water out of only one side of the chamber. During the dip, just after the contraction has finished, we instead see a negative pressure gradient inside the salp. This negative pressure gradient is the result of water still flowing out of the chamber due to inertia, but without any contraction to support the flow. This inversion of the pressure gradient is shown in figure 9.

However, this backwards thrust might not be a problem for real salps. The anterior siphon of a real salp is a one-way valve, which closes at over-pressure and opens at under-pressure. As such, the anterior siphon could open and equalize the pressure as soon as a negative pressure gradient begins to form, removing the risk for a substantial backwards thrust. To get a more realistic salp model it could therefore be important to model this valve accurately, instead of the crude contact model used in these experiments.

Another interesting aspect is the smaller oscillations in pressure shown at roughly 1.85s in figure 6. These oscillations is the result of the posterior siphon closing and the anterior siphon opening, resulting in a sudden closing of the pressure gradient at the posterior siphon due to the contact model. The sudden removal of the pressure gradient results in waves of pressure and an oscillating thrust. Another way to get a more realistic salp model it could therefore be to implement a gentler contact model that does not result in such pressure waves.

4.2 Thrust versus siphon diameter

In figure 7 we can see a clear exponential relationship between posterior siphon diameter and average thrust. We would expect the thrust to increase with smaller a diameter, since the thrust is a function of the flowrate and the velocity. The flowrate should remain constant regardless of the diameter, since the same volume is expelled in the same amount of time, but a smaller diameter requires a higher velocity to sustain this flowrate. However, it is not immediately clear why the relationship should be exponential, so further investigation into this relationship could be of interest.

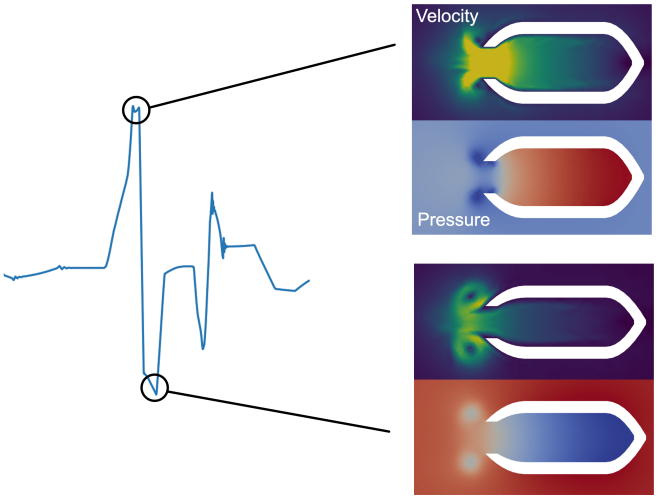

Figure 9: The pressure and velocity fields (right) corresponding to the peak and dip in the measured thrust (left). The inversion from a positive to a negative pressure gradient at the end of contraction can be seen.

4.3 Thrust versus chamber height

We see in figure 8 that the relationship between maximum chamber height and average thrust also appears to be exponential. Forward thrust improves drastically when the maximum chamber height increases, which is expected since a larger chamber increases both the outflow rate and outflow velocity (since a larger volume is expelled in the same amount of time). However, just as in the exploration between thrust versus siphon diameter, the reason for precisely an exponential relationship is not clear, so further investigation could be of interest.

5 Conclusion

The test case, consisting of a simulating a simplified 2D salp model, has been generally successful, with the parametric analysis showing reasonable results. Exponential relationships between dimensional parameters and thrust appears to be common.

Comparisons with previous studies were impeded by the lack of detailed information about the pulse cycle of salps measured and by the salp not being simulated in three dimensions. However, there are many opportunities for future, more detailed studies to add realism and create more comparable and applicable data. As such, numerical simulation could be a promising tool to study the propulsion of salps and complement real-world measurements, but more research is needed.

6 Future work

A natural extension of this project is to construct a more realistic model of the salp to allow for better comparisons with measurements from previous studies. To add realism, the salp could be modeled in three dimensions, with a less idealized and more realistic morphology. As mentioned previously, it could be important to accurately model the valve at the anterior siphon and to implement at contact model that does not result in pressure waves.

Another improvement would be to model a free-swimming salp. In this report, the thrust do not result in any movement of the salp, meaning the salp is stuck in a fixed position. This facilities comparisons with previous studies, where measurements have been taken with salps in a fixed position, but a free-swimming salp would better reflect a real-world scenario. Salp movement could be simulated while still keeping the salp centered in the mesh if the corresponding acceleration is imparted uniformly to the fluid in the opposite direction.

References

[1] K. Sutherland and L. Madin, "Comparative jet wake structure and swimming performance of salps," *The Journal of experimental biology*, vol. 213, pp. 2967–75, 09 2010.

[2] N. Henschke, J. D. Everett, A. J. Richardson, and I. M. Suthers, "Rethinking the role of salps in the ocean," *Trends in Ecology Evolution*, vol. 31, no. 9, pp. 720–733, 2016.

[3] L. P. Madin, "Aspects of jet propulsion in salps," *Canadian Journal of Zoology*, vol. 68, no. 4, pp. 765–777, 1990.

[4] P. Linden and J. Turner, "Optimal vortex rings and aquatic propulsion mechanisms," *J. Fluid Mech.*, vol. 427, 01 2001.

[5] F. Mbithi, "Design and evaluation of a propulsion system for small, compact, low-speed maneuvering underwater vehicles," 2014.

[6] A. Thomas, M. Milano, M. G'Sell, K. Fischer, and J. Burdick, "Synthetic jet propulsion for small underwater vehicles," in *Proceedings of the 2005 IEEE International Conference on Robotics and Automation*, pp. 181–187, 2005.

[7] M. Krieg and K. Mohseni, "Thrust characterization of a bioinspired vortex ring thruster for locomotion of underwater robots," *Oceanic Engineering, IEEE Journal of*, vol. 33, pp. 123 – 132, 05 2008.

[8] Q. Bone and E. R. Trueman, "Jet propulsion in salps," *Journal of Zoology*, vol. 201, no. 4, pp. 481–506, 1983.

[9] J. Hoffman, J. Jansson, N. Jansson, and R. V. De Abreu, "Towards a parameter-free method for high reynolds number turbulent flow simulation based on adaptive finite element approximation," *Computer Methods in Applied Mechanics and Engineering*, vol. 288, pp. 60–74, 2015.